Soil Dynamics and Earthquake Engineering 29 (2009) 382–393

Contents lists available at ScienceDirect

Soil Dynamics and Earthquake Engineering

journal homepage: www.elsevier.com/locate/soildyn

The role of strong motion rotations in the response of structures near earthquake faults

Mihailo D. Trifunac

Department of Civil Engineering, University of Southern California, Los Angeles, CA 90089, USA

ARTICLE INFO

Article history:
Received 30 October 2007
Received in revised form
28 March 2008
Accepted 6 April 2008

Keywords:
Strong earthquake rotations
Earthquake response of structures near faults

ABSTRACT

Early studies of earthquake strong motion assumed linear materials and small deformations. It was observed that under favorable conditions (long waves), the accompanying rotational motions are usually small, and so their effects could be neglected. In 1932, when Biot opted for the vibrational method of solution of the dynamic response problems [Trifunac MD. 75th anniversary of the response spectrum method—a historical review. Soil Dyn Earthquake Eng 2008 [in press].] in his formulation of the response spectrum concept, his choice of the discrete mathematical models of buildings further led to the conditions that did not explicitly require consideration of the rotations [Trifunac MD. Buildings as sources of rotational waves, Chapter I.5. In: Teisseyre R, Nagahama H, Majewski E, editors. Physics of asymmetric continua: extreme and fracture processes. Heidelberg, Germany: Springer; 2008 [in press].]. The engineering profession was not prepared in the 1930s and 1940s for Biot's new theory and first had to learn the basic dynamics of structures before it could question the wisdom and consequences of the vibrational versus the wave-propagation approaches to the solution. Also, there were too many other concerns, often caused by the modeling simplifications, that pushed the studies of the rotational motion further down to the low levels of priority. Even today, 40 years after the arrival of digital computers and the emergence of powerful numerical computational capabilities, which uncovered unexpectedly large families of chaotic solutions accompanying large deformations, as well as nonlinear response [Trifunac MD. Nonlinear problems in earthquake engineering. In: Springer's encyclopedia of complexity and system science, 2008 [in press] [94].], most researchers continue to ignore the role of rotations. Had Biot chosen the wave-propagation approach for the solution of the earthquake engineering problems in 1932, the "progress" might have been faster. The wave representation can be differentiated with respect to a space coordinate, giving the rotations at a point directly. In contrast, the lumped-mass models in the vibrational approach do not make this possible, and the closest one can come to considering rotations is in terms of average, per-floor rotation, or drift.

This paper reviews some elementary aspects of ground motion near faults and the resulting structural deformations in order to illustrate the role of the strong-motion rotations. We show rough estimates of how large such rotations can be, and we suggest how the profession might begin to study and interpret their consequences. Whether the aim is to understand why micro-tremors in metropolitan areas abound with high-frequency Rayleigh waves, why buildings rock and occasionally overturn during strong earthquake shaking, or why columns fail, we must consider the rotational components of ground and structural motions. Only then will we be able to understand and control the response to strong earthquake excitation.

1. Introduction

The selection of mathematical models for the dynamic analysis of structures influences and often dictates the method of solution. The physical nature of the models also influences the spatial and temporal details of the information that can be extracted from the computed response.

The contemporary form of the vibrational approach for solving linear dynamic response of multi-degree-of-freedom systems in earthquake engineering evolved from Biot's Ph.D. thesis [1], which dealt with the general theory of transient response. In Chapter II of his thesis, Biot introduced what would later become known as the response spectrum method (RSM), and he then fully developed the method in Biot [2,3]. Very little has changed since 1932, and earthquake engineers still follow the method and the representation he introduced 75 years ago [4].

In contrast to Biot's vibrational description of the response, in the following we consider elastic waves in homogeneous isotropic

E-mail address: trifunac@usc.edu

0267-7261/$ - see front matter © 2008 Elsevier Ltd. All rights reserved.
doi:10.1016/j.soildyn.2008.04.001

and elastic media using only the first-order linear theory of elasticity [5]. If nonlinear phenomena occur along the wave path, and if those are investigated, the engineering analysis is usually restricted to the response of soft soil deposits near the ground surface and to waves in the buildings, in terms of most elementary representations of nonlinear behavior of the material (e.g. [6,7]). More advanced representations of the material involve the microphysics of fracture and include the irreversible deformations from dislocations, disclinations, and micro-cracks [8]. However, in the following—the rotational strong motion in the response of the ground and of man-made structures—only the former, macroscopic representation will be considered.

Rotational components of strong motion always accompany the displacements induced by seismic waves, but only few attempts have been made to measure or estimate their properties and effects [9–24]. In linear elastic media, "point rotations" can be expressed by space derivatives of the displacements (e.g. [25]). Other contributions to rotational motion can result from the internal structure of the medium, non-symmetric processes of fracture, and friction [26]. Once generated, these additional rotational motions are believed to attenuate quickly, and so, to be studied experimentally, they have to be recorded in the near field [27]. Early measurements and calculations at teleseismic distances estimated rotations of ground motion to be smaller than about 10^{-6} rad [28–30].

"Average rotations" (rotation of a line connecting two moving points and separated by a distance that can be comparable to and longer than the representative wavelengths) can be computed from the differences in the recordings of two translational records from an array of stations on the ground surface [21,31–35] and in structures [36–38]. Such estimates approximate the average rotations over the distance separating the two translational records and may approximate the rotations at a point only for the wavelengths that are much longer than this separation distance. This is a limitation for the studies of point rotations of strong motion in the ground, in the structures, and in the flexible foundations of structures [37,39], but it is suitable, and in some cases it is desirable, for describing relative rotations in engineering analyses of buildings in terms of inter-story drifts [38].

In the following, we examine the amplitudes of early transient rotational motions at the earthquake source and cite examples of how those rotations have been used in computation of the response of structures. Throughout this paper we will rely on dimensional analysis and geometric features of the problem and will neither derive nor solve the governing equations of response. Those equations require specific mathematical models of structures and cannot be written in a form that would be valid for a general case. Therefore, the material presented in this paper can be viewed only as a qualitative experiment aimed at finding the functional relationships, orders of magnitude, and relative significance of the variables involved.

Finally, this presentation is neither meant to be comprehensive nor complete, and many studies and topics related to the rotational components of strong motion in structures and in the soil will not be considered [40]. Soil–structure interaction will not be considered, and only the nature of the ground motion in the vicinity of the moving faults will be addressed. Close to the faults, the rotational components of strong motion are expected to be large, and thus they can contribute most to the response of structures.

2. Sources of rotational motion

The elementary representation of the generation of seismic waves can be assumed to begin with kinematic description of faulting (e.g. [14,30,41], which then evolves with radiated waves, all in terms of the first-order linear theory of elasticity. In the following, as we analyze the rotational motions on the ground surface and in the response of man-made structures, only this macroscopic representation will be considered.

2.1. Earthquake source

Strong ground motion near faults is complicated by the irregular distribution of fault slip caused by non-uniform and asymmetric distribution of geologic rigidities surrounding the fault, non-uniform distribution of stress on the fault, and complex nonlinear processes that accompany faulting. Thus, it is not possible to predict the detailed nature of the near-fault ground motion. In the following, we adopt a qualitative approach and illustrate these motions by smooth displacements, which have representative average amplitudes and duration and which have been calibrated against the observed fault slip and the recorded strong motions in terms of their peak amplitudes in time and their spectral content [42,43].

Fig. 1 shows schematically a vertical strike-slip fault and two simple horizontal motions, d_N and d_F, which we adopt here to describe monotonic growth of the fault slip toward the permanent static offset, and a pulse, which, when near to a fault, may be perpendicular to the fault and could represent a failure of a nearby asperity or passage of dislocation under or past the observation point. By appropriate geometrical transformations, the above examples can be generalized to describe any components of motion when faults have arbitrary orientation, but in the following we will, for simplicity, discuss only the above example of a vertical strike-slip fault. Furthermore, for arbitrary fault orientation, static fault offset will lead also to permanent tilting of the ground surface, and this will result in the corresponding tilting of structures. Analysis of the consequences of this tilting on the response of structures is beyond the scope of this paper.

For a pulse, we adopt (Fig. 1, center):

$$d_F(t) = A_F t\, e^{-\alpha_F t}, \tag{1}$$

where average values of A_F and α_F, for different earthquake magnitudes, are shown in Table 1 [42]. Because the strong-motion data are abundant only up to about $M = 6.5$, the values of the scaling coefficients for $M = 7$ and 8 in Tables 1 and 2 are placed in parentheses to emphasize that those are based on extrapolation. For the fault-parallel displacement, we consider (Fig. 1, bottom):

$$d_N(t) = \frac{A_N}{2}(1 - e^{-t/\tau_N}), \tag{2}$$

where average values of A_N and τ_N, for different earthquake magnitudes, are shown in Table 2.

The amplitudes of d_F and d_N can be related to many regression analyses of recorded peak displacements at various distances from the fault and in terms of the observed surface expressions of fault slip. The latter are traditionally presented as average dislocation amplitudes, $\bar{u}$, and are related to d_N, as $\bar{u} = 2d_N$ (see Fig. 1, top).

Fig. 2 summarizes the trends of average dislocation amplitudes, $\bar{u} = 2d_N$, versus magnitude M, which corresponds to the local Richter magnitude, M_L, when M is smaller than about 6.5, and to surface wave magnitude, M_S, for larger magnitudes [44]. Various symbols show the results extracted from the strong-motion studies of selected earthquakes, while the two gray zones outline the boundaries of the 80% confidence interval (bounded by $p = 0.1$ and 0.9, where p is the probability of not exceeding) for the amplitudes of $\bar{u} = 2d_N$ based on the family of four regression models (G4RM) that describe attenuation of strong-motion peak displacements [42]. The dashed line in Fig. 2 shows the

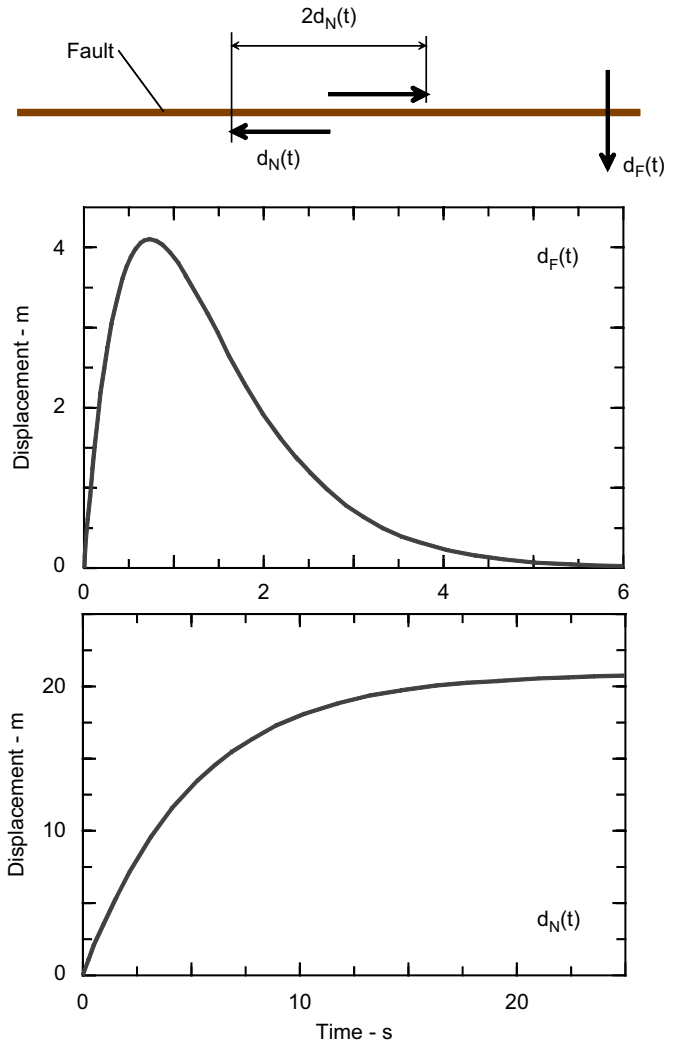

Fig. 1. Fault-parallel, $d_N(t)$, and fault-normal (pulse), $d_F(t)$, displacements near vertical strike-slip fault, adopted to represent near-source motions in this study.

Table 1
Characteristics of pulse displacement [42]

M (magnitude)	α_F (s^{-1})	A_F (cm/s)	$d_{F,max}$ (cm)	$\dot{d}_{F,max}$ (cm/s)
4	14.04	56.48	1.48	56.48
5	7.90	151.61	7.06	151.61
6	4.44	546.97	45.32	546.97
7	(2.50)	(860.34)	(126.6)	(860.34)
8	(1.40)	(1560.29)	(410.0)	(1560.29)

Table 2
Characteristics of near-field displacement [42]

M (magnitude)	τ_N (s)	A_N (cm)	$d_{N,max}$ (cm)	$\dot{d}_{N,max}$ (cm/s)
4	0.55	4.9	2.45	4.45
5	1.2	29.2	14.6	12.17
6	1.8	245.5	122.75	68.19
7	(3.0)	(1288.0)	(644.0)	(214.7)
8	(5.0)	(4169.0)	(2084.5)	(416.9)

amplitudes of $2d_{N,max}$, as given in Table 2. It can be seen that the agreement is satisfactory.

An important physical property of d_F and d_N functions is their initial velocity. It can be shown that $\dot{d}_F \sim \sigma\beta/\mu_s$, where σ is the effective stress (~stress drop) on the fault surface, β is the velocity of shear waves in the fault zone, and μ_s is the rigidity of rocks surrounding the fault. For $\dot{d}_N$, it can be shown that $\dot{d}_N = 0.5\,C_0\sigma\beta/\mu_s$ at $t = 0$, where typical values of C_0 are 0.6, 0.65, 1.00, 1.52, and 1.52 for $M = 4$, 5, 6, 7, and 8, respectively [45]. The largest peak velocities of strong ground motion observed so far are in the range of 200 cm/s (170 cm/s, 5–20 km above the fault of the 1994 Northridge, California earthquake ($M_L = 6.4$, $M_W = 6.7$) [46] and 229 cm/s at station TCU068, near the end of surface expression of the Che-lungpu fault, during the 1999 Chi-Chi, Taiwan earthquake ($M_L = 7.3$, $M_W = 7.6$) [47].

Because there are no strong-motion measurements of peak ground velocity at the fault surface, the peak velocities $\dot{d}_F$ and $\dot{d}_N$ can be evaluated only indirectly in terms of σ, for example. The accuracy of the stress estimates depends upon the assumptions and methods used in the interpretation of recorded strong-motion records and is typically about one order of magnitude. Therefore, by solving the above equations for σ we can use $\sigma \sim 2\mu_s\dot{d}_N/\beta C_0$ (dotted lines in Fig. 3) and $\sigma \sim \mu_s\dot{d}_F/\beta$ (continuous lines in Fig. 3) to check their consistency with other published estimates of σ. Fig. 3 shows this comparison for a typical range of values of μ_s and β.

Fig. 3 also describes the order of magnitude of the peak rotational ground motions at the fault (assuming the phase velocity $c_g \sim 1$ km/s) and the order of magnitude of the expected drift in the buildings (assuming that a typical value of the phase velocity c_b in the building is ~0.1 km/s (e.g. [48]). It can be seen that for the buildings located at or very close to surface faults, large initial velocities $\sigma\beta/\mu_s$, associated with either d_F or d_N, will begin to damage the buildings for intermediate and large magnitudes. As the distance between the fault and the recording site increases, attenuation and dispersion will diminish and smooth out the sharp jump in initial strong-motion velocity $\sigma\beta/\mu_s$. Fig. 3 includes four such examples of peak ground velocity, recorded during the Parkfield, 1966, San Fernando, 1971, Northridge, 1994, and Chi-Chi, 1999, earthquakes. These examples illustrate the motions recorded close to the moving faults but may be as much as 20 km away from the fault slip (asperity) producing those peak velocities.

For the examples of d_F and d_N in this work, there is a Dirac delta function in accelerations at time zero. In the observed motions, because the waves arrive through sediments and soil with finite strength, this will correspond to large but not infinite accelerations [49]. Fig. 4 (top) shows one of the early examples of the ground displacement, perpendicular to the fault, recorded during the 1966 Parkfield, CA earthquake [50]. This displacement, computed by double integration from the recorded accelerogram [52] is used to illustrate the near-fault "pulse-like" ground motion, which we approximate here by d_F (shown in Fig. 1, middle). Fig. 4 (bottom) shows the ground displacement computed during the 1971 San Fernando, CA earthquake [53]. This displacement has been high-pass filtered by routine data-processing methods [54,55], and therefore it does not contain periods of motion longer than 15 s. However, in spite of this high-pass filtering, it clearly shows two episodes of permanent ground displacements, starting near 2.5 and 7 s [51].

2.2. Wave propagation and nonlinear site response

Translational and rotational components of strong motion that are radiated from an earthquake source change along the propagation path through interference, focusing, scattering, and

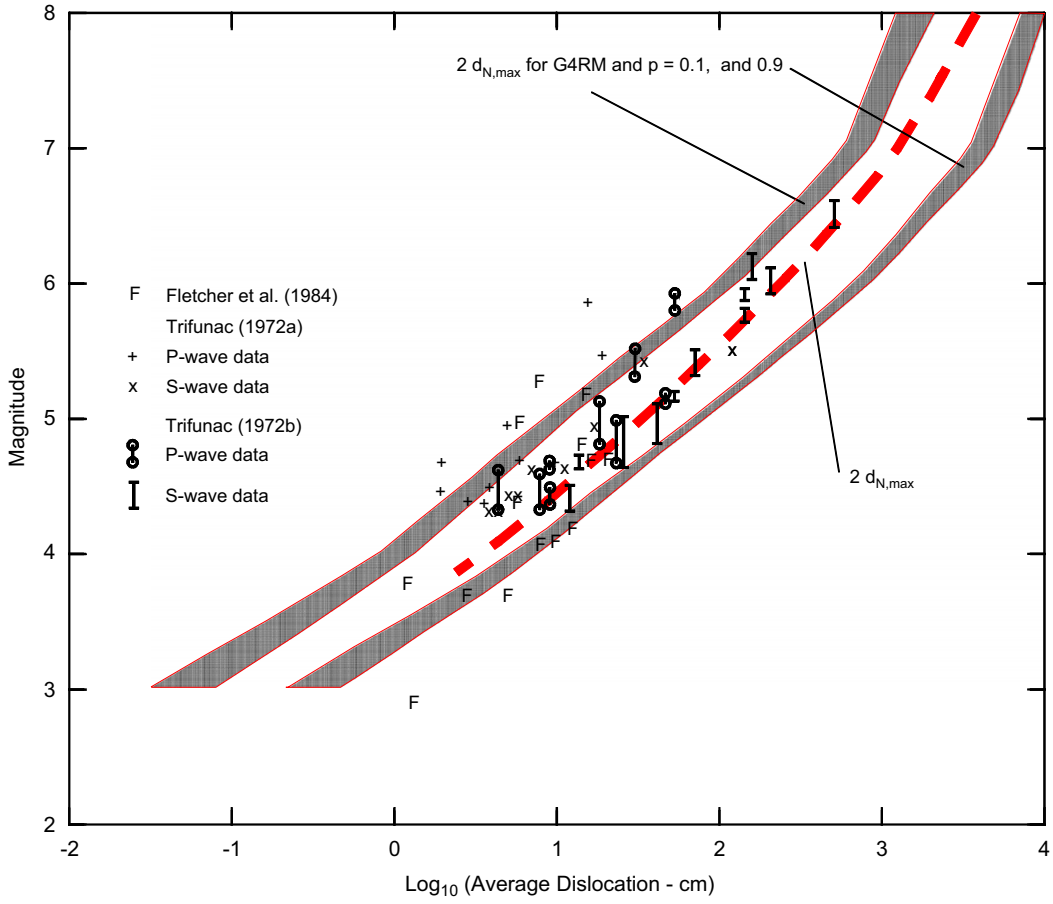

Fig. 2. Comparison of the average dislocation amplitudes on the fault, $\bar{u} = 2d_{N,max}$, evaluated in several spectral analyses of the recorded strong ground motion (different symbols), with the amplitudes of $d_{N,max}$ (Table 2) adopted for scaling $d_N(t)$ in this paper (dashed line) [92,93].

diffraction. For example, reflection of plane P and SV waves from half space can lead to large displacement amplitudes for incident angles between 30° and 43°, but the associated rotations (rocking for P and SV waves, and torsion for SH waves) change monotonically and do not lead to large amplifications [25,56]. Scattering and diffraction of plane waves from topographic features can lead to focusing and to amplification for both displacements and rotations [57].

The estimates of peak ground rotations, via peak velocities $\dot{d}_F$ and $\dot{d}_N$ and stress drop estimates on the fault plane, shown in Fig. 3, are based on idealized linear representation of wave motion in the homogeneous and isotropic medium, and on the rough assumption that the "representative" phase velocities in the ground can be approximated by an equivalent single value $c_g \sim 1$ km/s. For large amplitudes of strong motion, surface soil, sediments, and weathered rock will undergo nonlinear deformations, which will further increase the amplitudes and the complexity of the observed ground deformations and rotations. This can be illustrated for the accelerograph site at the Pacoima Dam, CA. During the 1971 San Fernando ($M_L = 6.6$) earthquake, peak ground velocity of 115 cm/s in the N16°W direction was recorded at this site [53] by an AR-240 accelerograph, which was located on a rocky spine adjacent to the southern dam abutment. Extensive cracking of the gneissic granite-diorite and a small rock slide were observed adjacent to the instrument housing after the earthquake (Fig. 5 in [53]. After the earthquake, the instrument base was tilted to NW permanently, through an angle of about 0.5°. This permanent tilt was measured from the adjustments required to re-level the accelerograph. It occurred during the strong shaking of the main earthquake event, and having exceeded the tilt (~0.003 rad, or 0.17°) required to close the gap (0.05 cm) of the vertical starter pendulum (about 18 cm long), it resulted in continuous operation of the accelerograph, until it spent all available recording paper [58]. This accelerograph site was shaken again, during the 1994 Northridge ($M_L = 6.4$, $M_W = 6.7$) earthquake and experienced permanent tilt of about 3.5° in the NE direction [17].

The permanent tilts from the above example are shown in Fig. 3 to illustrate how much larger can be the rotations associated with nonlinear response of near-surface deposits. The lessons from this example cannot be generalized to quantitative predictions for other sites, as nonlinear response depends on numerous site-specific and excitation-specific factors. Nevertheless, this example reminds us to examine cautiously the conclusions that are often made on the basis of numerical simulations of linear theory alone. In their study of the simulations of the San Fernando earthquake, Bouchon and Aki [30], for example, found the maximum tilt a few kilometers from the fault to be only about 0.0007 rad (Fig. 3) and concluded that its contribution to earthquake damage is small compared with the contribution from strong-motion translations. A comparison with the observed tilts at the Pacoima dam accelerograph site suggests that the linear simulations of rotational strong-motion amplitudes, as in Bouchon and Aki's paper, can underestimate the total strong-motion rotations by orders of magnitude.

While studying large rotational velocities recorded a few kilometers away from an earthquake swarm in 1997, offshore from the Izu peninsula in Japan, Takeo [19,20] showed that they were several times larger than the rotational velocities in the numerical simulations by Bouchon and Aki [30]. However, the

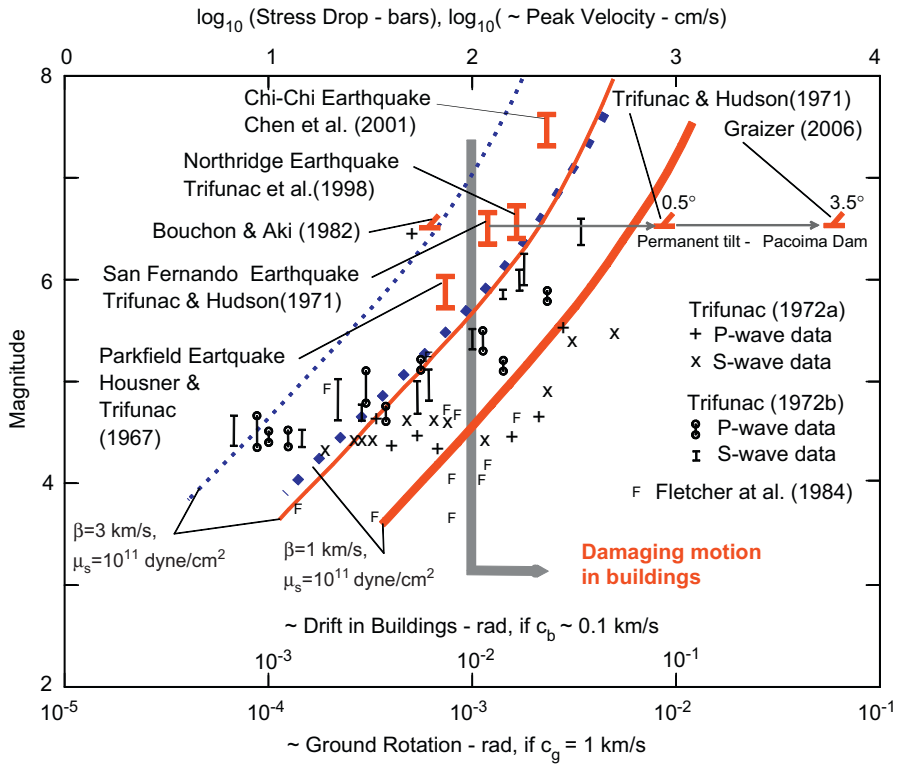

Fig. 3. Comparison of stress drop determined from near-field recordings of strong motion (different symbols), with the stress drop associated with $\dot{d}_F$ (solid lines, Table 1) and $\dot{d}_N$ (dotted lines, Table 2) as used in this paper. Also shown are the order-of-magnitude estimates of peak rotational ground motions at the fault (assuming the phase velocity c_g~1 km/s), and the order of magnitude of the expected drift in the buildings excited by the d_F and d_N displacements (assuming that a typical value of the phase velocity c_b in the building is 0.1 km/s).

earthquakes that he recorded were at larger epicentral distance and had two orders of magnitude smaller seismic moments than the corresponding earthquakes in the simulation used by Bouchon and Aki [30]. Takeo [20] proposed that "one possible answer is that the large rotational velocities are caused by heterogeneity of slip velocity on the fault," which is typically excluded in most numerical simulations. Takeo and Ito [59] derived a general expression for rotational velocities of seismic waves in terms of additional torsional and curvature tensors at the earthquake source and could explain the observations, but this required going beyond the usual formulation of the linear theory, which is used in common forward simulations. Takeo's (2006) peak tilts cannot be included for comparison with other trends shown in Fig. 3 because, with the limited sampling rate of 10 Hz and significant frequency content in the recorded rotational velocities only a little lower than 10 Hz, Takeo could not calculate the peak tilts.

As the above examples illustrate, beyond the results of linear theory, in the near field, the nonlinear response of soil, and ultimately soil failure and liquefaction, can lead to large transient and permanent rotations. Four types of ground failure, for example, can follow liquefaction: lateral spreading, ground oscillations, flow failure, and loss of bearing strength. *Lateral spreads* involve displacements of surface blocks of sediments facilitated by liquefaction in a subsurface layer. This type of failure may occur on slopes of up to 3° and is particularly destructive to pipelines, bridge piers, and other long and shallow structures situated in flood plain areas adjacent to rivers. *Ground oscillations* occur when the slopes are too small to result in lateral spreads following liquefaction at depth. The overlying surface blocks break one from another and then oscillate on liquefied substrate. *Flow failures* are a more catastrophic form of material transport and usually occur on slopes greater than 3°. The flow consists of liquefied soil and blocks of intact material riding on and with liquefied substrate on land or under the sea (e.g. at Seward and Valdez during the 1964 Alaska earthquake; [60]. *Loss of bearing strength* can occur when the soil liquefies under structures. The buildings can settle, tip, or float upward if the structure is buoyant. The accompanying motions lead to large transient and permanent rotations, which so far have been neither evaluated through simulation nor recorded by strong-motion instruments.

2.3. Asymmetry of support

Most man-made structures are built above the ground and can be tens of meters to several hundreds of meters high. Supported asymmetrically at their base, with their center of gravity near mid-height, they undergo rocking motions when excited by earthquakes, strong winds, and man-made transient and steady excitations. Through the rocking compliance, the soil–structure interaction then acts as a mechanism for conversion of the incident-wave energy into rotational motions of the foundation, which then radiate this wave energy back into the soil [61]. During earthquake and ambient noise (micro-seisms and micro-tremor) excitations, the incident waves are scattered and diffracted by the foundation–soil interface, and together with the waves generated by the soil–structure interaction radiate rotational motions back into the soil. During wind and man-made excitation, a part of the wave energy in the building is converted into rotational excitation of the soil, and rotational motion of the ground accompanying the response of "large" buildings can be a significant factor for excitation of nearby "small" structures [61]. The early work on the waves created by soil–structure interaction dates back to the 1930s [62,63] and the 1940s [64].

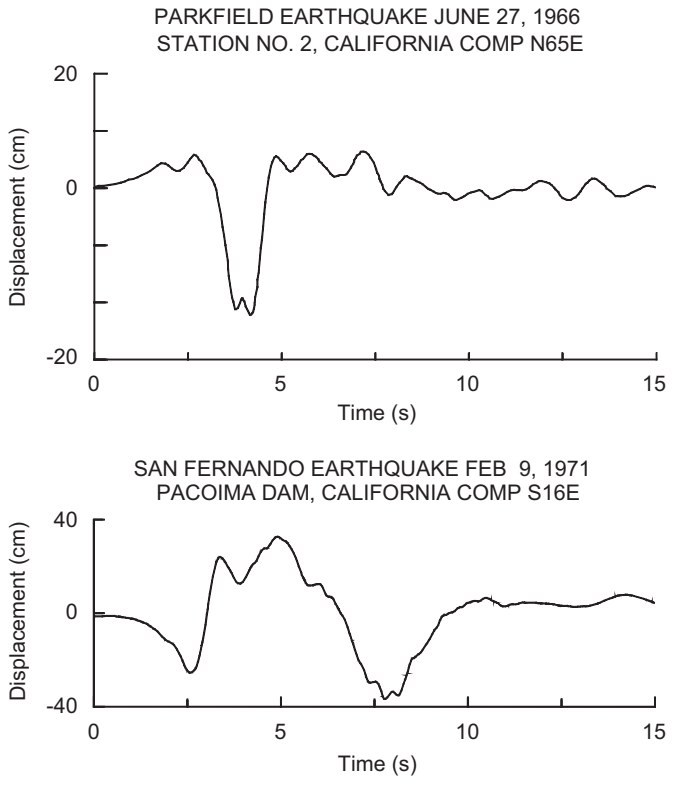

Fig. 4. Top: ground displacement (resembling d_F), perpendicular to the fault strike, about 10 km southeast, and 3 km above the southeastern end of the fault slip, on a vertical strike-slip fault, during the 1996 Parkfield, CA earthquake [50]. Bottom: ground displacement (resembling two episodes of d_N) recorded near the center and several kilometers above the thrust fault that ruptured during the 1971 San Fernando, CA earthquake [51].

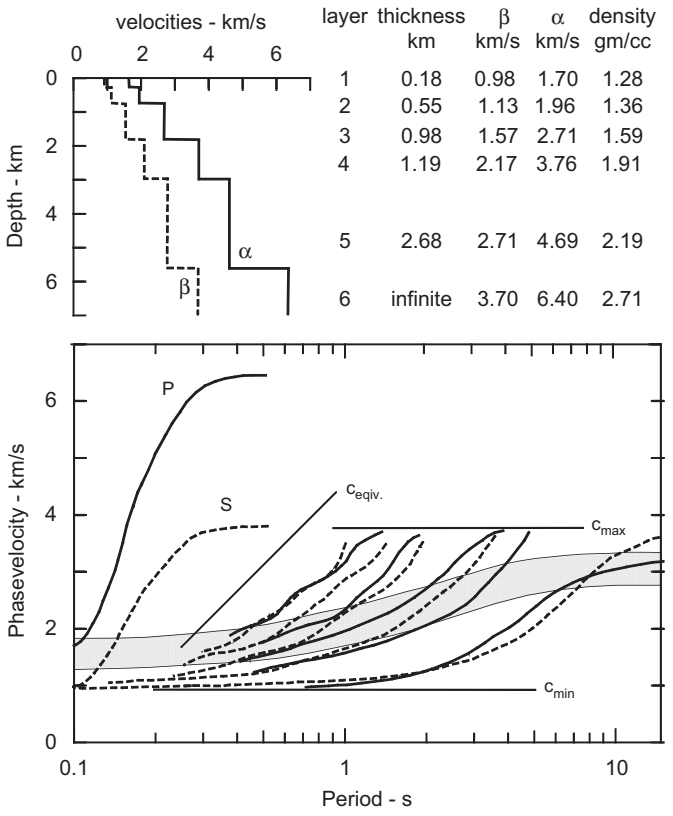

Fig. 5. (Top) Typical variation of P-wave (α) and S-wave (β) velocities versus depth in El Centro, Imperial Valley, CA; and (bottom) the corresponding Love (dashed lines) and Rayleigh (full lines) phase velocities (redrawn from Ref. [10].

2.4. Artificial strong motion

In the absence of recorded rotational components of strong ground motion, it has been necessary for engineering studies of response to have at least preliminary and physically realistic simulations of such motions [65,66]. The method of Lee and Trifunac meets some of these requirements in that it generates torsional and rocking accelerograms using an exact analytical method, if it is accepted that (1) the motion occurs in a linear-elastic, layered half-space, and (2) synthetic ground motion can be represented by body P and SV waves and by Rayleigh surface waves for rocking [11], and by body SH and surface Love waves for torsion [10]. This method has been extended to predict the associated strains [67] and curvatures near the ground surface [68] during passage of seismic waves.

In the following, to provide a basis for approximate representation of rotations in terms of peak ground velocity, we illustrate the method of Trifunac and Lee for torsional ground motion. Mutatis mutandis, the rocking of ground motion can be expressed in a similar way [11]. The rotation of the ground surface about vertical axis z associated with horizontal motions u_x and u_y in the horizontal x- and y-directions is equal to

$$\phi = \frac{\partial u_y}{\partial x} - \frac{\partial u_x}{\partial y}. \tag{3}$$

In the following example, we assume the presence of SH and Love waves only, propagating in the x-direction (so that $u_x = 0$), and we express the rotation ϕ by [69]

$$\phi = \frac{\partial u_y}{\partial x}. \tag{4}$$

For harmonic-wave motion, $u_y = A\,e^{i\omega(t-(x/c_x))}$ and $\phi = -A(\omega/c_x)\,e^{i\omega(t-(x/c_x))}$, and for particle velocity $v_y = \partial u_y/\partial t = A\omega\,e^{i\omega(t-(x/c_x))}$ this gives $\phi = -v_y/c_x$, where c_x is the corresponding phase velocity. For strong earthquake ground motion, which is a superposition of many harmonic waves with different phase velocities, we assume that the rotation $\phi(t)$ in Eq. (4) can be approximated by $\phi_0(t)$:

$$\phi_0(t) = \frac{-v_y(t)}{c_{\text{eqiv.}}}, \tag{5}$$

where $c_{\text{eqiv.}}$ is some "average" or "representative" phase velocity, $c_{\min} < c_{\text{eqiv.}} < c_{\max}$, and $c_{\min}$ and $c_{\max}$ are the minimum and maximum phase velocities at a site with parallel layers (Fig. 5).

Approximation in terms of Eq. (5) cannot be verified by comparison with recorded data because strong-motion torsional accelerograms $\ddot{\phi}(t)$ and velocities $\dot{\phi}(t)$ have not been recorded thus far [70]. However, for a layered half space and linear wave propagation, this approximation can be tested by comparison with synthetically computed rotation and velocity [10,25,71]. We illustrate this by considering artificial translational and torsional accelerograms computed for a hypothetical earthquake with magnitude $M = 6.5$ at epicentral distance $R = 10$ km, and for horizontal and torsional motions evaluated for a layered half space model at the El Centro, CA site [10]. This comparison is shown in Fig. 6, where $v(t)$ and $\phi(t)$ are computed by a synthesis of surface and body waves. It is seen from this example that Eq. (5) can represent a reasonable approximation, provided a suitable phase velocity $c_{\text{eqiv.}}$ can be chosen.

It can be seen from Fig. 6 that for the long-period components ($T > 3$ s) $v(t)$ and $\phi(t)$ agree well, when $c_{\text{eqiv.}} \sim 3000$ m/s. For intermediate- and short-period ($T < 1$ s) motions, however, $c_{\text{eqiv.}}$

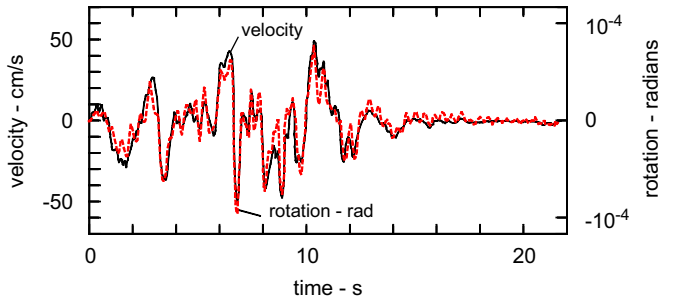

Fig. 6. Comparison of synthetic ground velocity and the associated torsional rotation (modified from Ref. [10]).

should be smaller, decreasing from $c_{\text{eqiv.}}\sim$2000 m/s near $T=1$ s toward $c_{\text{eqiv.}}=1$ km/s as $T\to 0$. The trend of these changes in $c_{\text{eqiv.}}$ is illustrated by a shaded zone in Fig. 5, between 1.5 and 3 km/s for periods between 0.1 and 15 s.

2.5. Peak ground velocity near faults

Spectral amplitudes of recorded strong motion have been investigated in some detail in the frequency range from 25 to 0.1 Hz [42]. For frequencies smaller than 0.1–1 Hz, in the near field, Fourier spectrum amplitudes of strong-motion acceleration are expected to have the form:

$$\text{FS}_{\text{NF}}(\omega)\sim\omega[(\omega\tau_0)^2+1]^{-1/2}, \tag{6}$$

where duration of faulting is

$$\tau_0\sim\frac{L}{v}+\frac{0.5W}{\beta}, \tag{7}$$

and where L and W are fault length and width, v is the velocity with which the dislocation is spreading along the fault length, and β is the velocity of shear waves in the source region.

One corner frequency, in the near-field spectra of strong-motion accelerations is then defined by $f_1=1/\tau_0$. In the far field, the average shape of the body-wave spectra of strong-motion acceleration can be described by [42]

$$\text{FS}_{\text{FF}}(\omega)\sim\omega^2[1+\omega^2(2\pi f_2)^{-2}]^{-1/2}[1+\omega(2\pi f_1)^{-1}]^{-1}, \tag{8}$$

where

$$f_2\sim\frac{2.2}{W} \tag{9}$$

and $1/f_2$ approximates the time required for the dislocation to spread over the fault width W.

Corner frequencies f_1 and f_2 cannot be determined from strong-motion data alone, but their estimates can be obtained by extrapolation of empirical amplitudes of strong motion for $f<0.1$ Hz and by fitting and interpolation to the known data on the fault length L, width W, dislocation amplitudes $\bar{u}$, and the stress drop [72].

Assuming that in the beginning the dislocation starts to grow linearly with time, as in $\sigma\beta t/\mu_s$ (where σ is stress drop, β is the shear-wave velocity, and μ_s is the rigidity in the source region), until it reaches the final dislocation, $\bar{u}/2$, we can approximate the dislocation rise time T_0 by

$$T_0\sim\frac{\bar{u}\mu_s}{2\sigma\beta}. \tag{10}$$

For a sudden constant shear-stress drop σ, where the stress vector is in the fault plane, on what at first appears as an infinite fault plane, the fault begins to move as $\sigma\beta t/\mu_s$ until the dislocation approaches the fault ends. Diffraction around the fault ends and complexities of nonlinear deformation in the fault zone then begin to slow down this displacement until it eventually reaches its permanent static value, $\bar{u}/2$.

Table 3
Average stress drop (bars) and dislocation rise time T_0 (s)

M (magnitude)	$\bar{\sigma}$ (bars)[a]	T_0 (s)[a]
4	20.0	0.31
5	50.0	0.73
6	100.0	1.6
7	160.0	5.4

[a] From Trifunac [42].

Table 4
Average velocity at fault surface if rise time is T_0 or $1/f_2$

M (magnitude)	$\bar{u}/(2T_0)$ (cm/s)	$\bar{u}f_2/2$ (cm/s)	T_0 (s)	f_2 (Hz)
4	4–9	1.7–9	0.31	1.4–3.2
5	17–22	9–20	0.73	0.74–1.2
6	72–90	58–101	1.6	0.51–0.70
7	104–157	179–332	5.4	0.32–0.39

For $\mu_s/\beta\sim0.3\times10^6$ dyne s/cm^3 and for average $\bar{u}$ and $\bar{\sigma}$ versus magnitude, T_0 can be computed and is shown in Table 3. Table 4 then shows two estimates of the average dislocation velocity during its rise time, equal to T_0 or $\sim1/f_2$. For independently evaluated T_0 and f_2, the estimates are given by $\bar{u}/(2T_0)$ and $\bar{u}f_2/2$. Peak ground velocity will be larger, particularly during the early phases of the dislocation growth—i.e. during energy release on near asperities—and will subside for $t\gg T_0$. Fig. 7 compares the estimates of average peak velocities, based on $\bar{u}/(2T_0)$ and $\bar{u}f_2/2$ with average peak ground velocity, at zero epicentral distance, computed from regression analyses of peak velocities derived from recorded and integrated accelerograms [73]. The line with short dashes represents average peak velocities expected at sites on sediments ($s=0$), and the line with long dashes shows the same, but for the sites on the basement rock ($s=2$). It is seen that the agreement between these rather different estimates is fair.

Fig. 7 also shows three measured peak velocities, which are among the largest velocities of strong ground motion observed so far and are relatively close to active faults (for Parkfield, CA earthquake of 1966; Northridge, CA earthquake of 1994; and Chi-Chi earthquake of 1999). For these three examples, the recording stations were at some distance from the moving dislocations, and therefore the peak velocities on the fault surface were larger. This is implied in Fig. 7 by arrows at points 1–3.

Fig. 7 also shows the estimates of $\dot{d}_{\text{F,max}}$ based on the pulse characteristics shown in Table 1. These velocities are consistent with the large stress-drop estimates illustrated in Fig. 3 and with the peak velocities recorded during the Parkfield 1966, and Northridge 1994 earthquakes (points 1 and 2). A small surface offset was observed near station no. 2, where this peak velocity was recorded, following the Parkfield 1966 earthquake. However, later studies have shown that the main rupture was 10–20 km north of station no. 2, on a buried fault, which extended from about 3 to 9 km below the surface [50]. During the Northridge earthquake, the main fault slip also did not reach the surface, and the dislocations leading to the observed peak velocity of about 170 cm/s at the Rinaldi Receiving Station were at least 5–20 km below the accelerograph site.

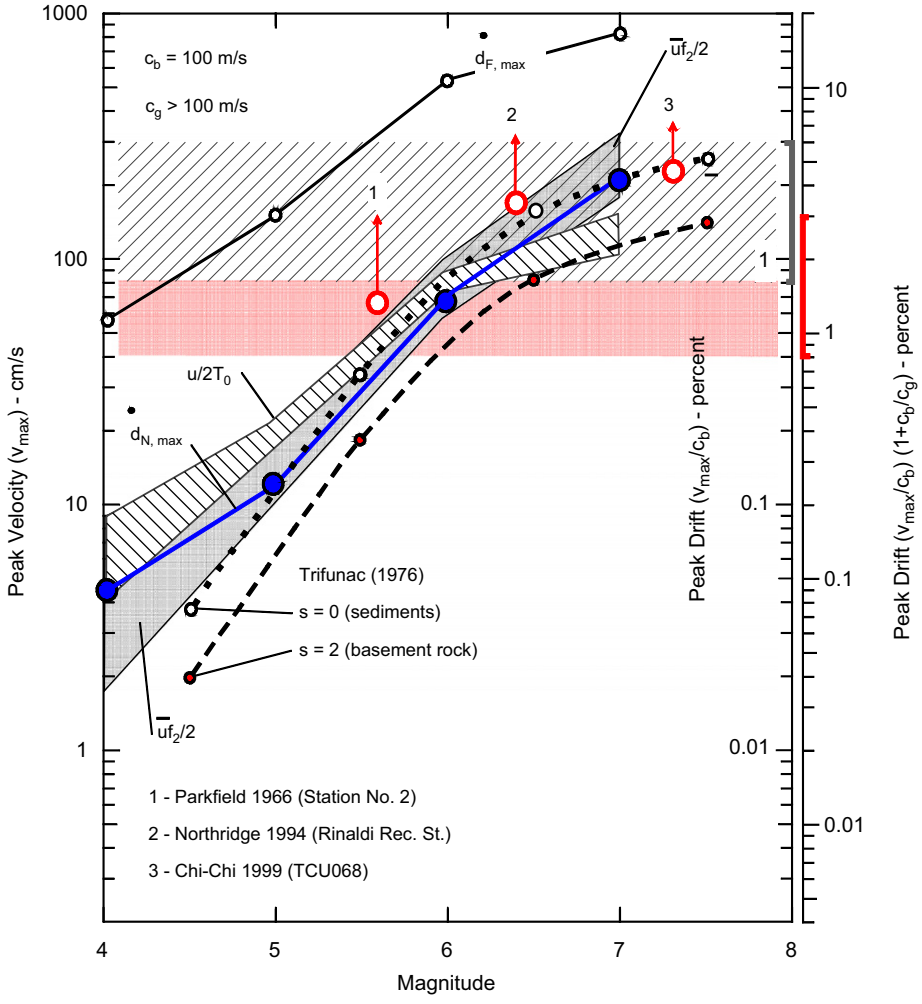

Fig. 7. Comparison of peak ground velocities (left vertical sale) based on (1) the initial slopes of the d_F and d_N displacements at the fault surface, (2) estimates of average rise time of dislocations ($\bar{u}/(2T_0)$ and $\bar{u}f_2/2$), and (3) empirical scaling equations extrapolated back to the fault surface at sites on sediments ($s=0$) and on the basement rock ($s=2$). The right-hand scale shows the range of approximate drift amplitudes in simple buildings, for $c_b \ll c_g$ and for $c_b \sim c_g$. Three examples of large peak velocities, recorded close to the fault surface, are shown for the Parkfield, Norhridge, and Chi-Chi earthquakes.

3. Structural response

In terms of the classical earthquake engineering approach, when the structure is represented by as SDOF system attached to the ground at a point, strong-motion translations and rotations are specified at the same point, and the governing differential equations include rotations as additional terms in the right-hand side, together with other forcing functions [23,24,74]. How the rotational components of strong ground motion will contribute to the response of extended structures with multiple supports will depend in a complicated way on the geometry of each structure, its structural system, its relative rigidity, the role of soil–structure interaction, and the composition and arrival angles of the incident earthquake waves. It will also depend on the plan dimensions of the structure, and on the nature of its connections to the ground. A dam, a bridge, or a building, for example, will respond to differential ground motions and rotations in very different ways [75–79]. A discussion of all these possibilities is beyond the scope of this paper, so here we only illustrate the role of the rotational excitation for a simple building supported by a flexible foundation. We also assume that the effects of soil–structure interaction are not present, and we consider an example of excitation by classical Rayleigh waves in the homogeneous half space only (Fig. 8). Finally, we ignore the dynamics part of the problem and consider only the pseudo-static deformations.

In Fig. 8, the ground surface is shown, at an instant, deformed by the passage of a Rayleigh wave, propagating from left to right, with phase velocity c_g. The surface displacement is characterized by particle motion along a retrograde ellipse, the principal larger axis of which is oriented in the vertical direction. We assume that in the instant shown the building is connected to the ground at point B. At this instant, the building foundation is forced to move to the right by displacement u_g and velocity v_g, and it experiences clockwise rocking of the ground with amplitude $\sim v_g/c_g$. For a building represented by a wide shear beam that is experiencing linear deformations only, the average drift will then be $v_g/c_b+v_g/c_g$ or $v_g(1+c_b/c_g)/c_b$, with the maximum value of $v_{max}(1+c_b/c_g)/c_b$. A typical value for c_b is of the order 0.1 km/s. The representative value of c_g will depend upon the source to station distance, the geometry of the medium through which the waves propagate, the composition of the wave train, and the distribution of wave velocities with depth, and it can be in the range from, say, 0.1 to more than 3 km/s. Consequently, the total drift in the building will be in the range between v_{max}/c_b (when $c_b \ll c_g$) and $2v_{max}/c_b$ (when $c_b \sim c_g$). These two extreme cases are illustrated in Fig. 7 by two vertical scales, on the right side. It is seen that the ground rocking

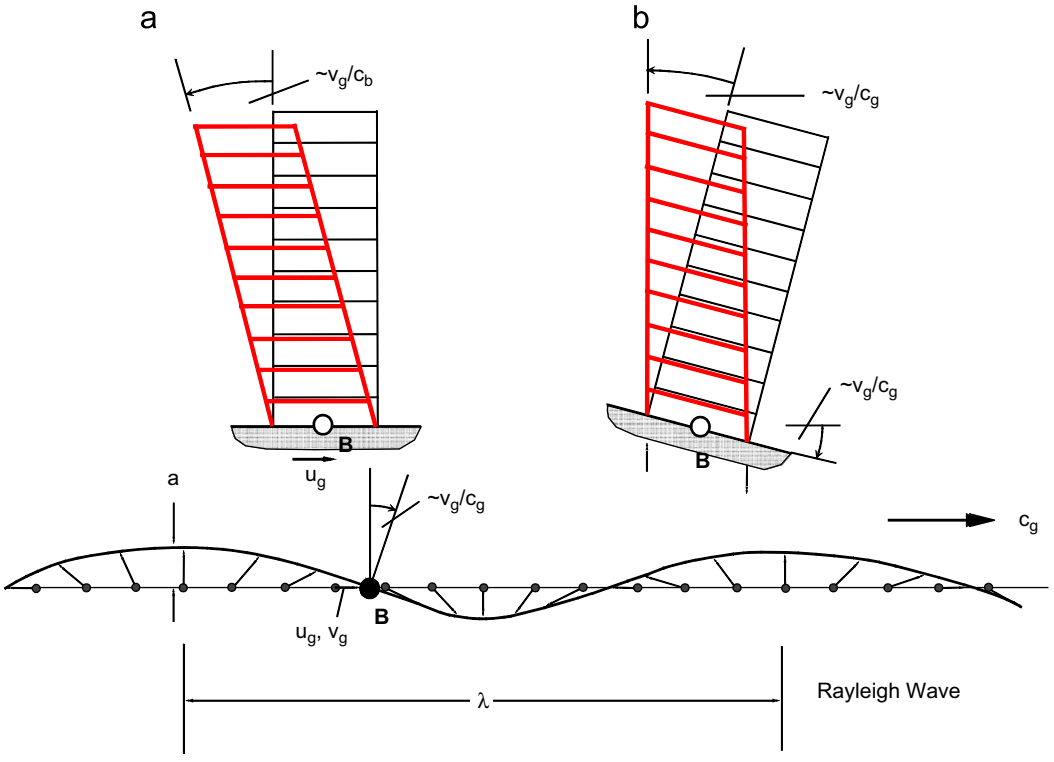

Fig. 8. Geometric interpretation of how horizontal translation and rocking can contribute to the total drift in a simple building during passage of a Rayleigh wave.

Table 5
Drift ratio (%) limits associated with various damage levels[a]

State of damage	Ductile MRF	Non-ductile MRF	MRF with infills	Ductile walls	Squat walls
No damage	<0.2	<0.1	<0.1	<0.2	<0.1
Repairable damage	0.4	0.2	0.2	0.4	0.2
Light/moderate	<1.0	<0.5	<0.4	<0.8	<0.4
Irreparable damage (>yield point)	>1.0	>0.5	>0.4	>0.8	>0.4
Severe damage–life safe–partial collapse	1.8	0.8	0.7	1.5	0.7
Collapse	>3.0	>1.0	>0.8	>2.5	>0.8

[a] Ghobarah [80].

will approximately double the drift amplitudes (for structures supported by soft sediment and soil layers, such as Mexico City) (right scale), while its role will be small for geologically stiff sites when $c_b \ll c_g$ (left scale). At the fault, the drift will exceed the typical design levels for magnitudes larger than 4–5. At the sites 50–100 km away from the fault, even for the largest levels of shaking, attenuation and geometric spreading will diminish v_{max} enough to produce drifts of less than about 1%.

3.1. Drifts in structural response

Most design codes specify the largest allowable drifts for the design of structures that are expected to experience dynamic loads. In general, the allowable drifts depend upon the structural material and the structural system. Because most design procedures formally follow some simplified "linear" theory of response, selection of allowable drifts and of allowable stresses is usually based on complex empirical evaluation of the expected nonlinear capacities of the structural system. Laboratory experiments on structural members and observations of buildings damaged by earthquake shaking are then used to evaluate, a posteriori, whether the design loads were adequate and how they should be updated based on actual experience.

Scatter in the observed drift amplitudes is considerable for the data based on the response calculations, for the data from laboratory experiments, and from the observations of the full-scale response [38]. The variety of structural models, the numerous simplifications in the modeling, and the incompleteness in the recording systems [37,70] all contribute to the uncertainty of the estimates and to the large scatter when the results are compared for many buildings. Table 5 illustrates the variation of drift amplitudes, in the range from no damage to collapse, for five structural systems (ductile moment resistant frames MRF, non-ductile MRF, MRF with infill walls, ductile walls, and squat walls [80]). It can be seen that damage begins to occur for drifts less than 0.1–0.2%, which corresponds to excitation with peak ground velocities larger than 10–20 cm/s. This is in good agreement with the simplified classical criteria for the threshold of damage [81]. These criteria were originally developed to describe damage to buildings from vibrations caused by blasting. Duvall and Fogelson found that safe motions are characterized by peak velocities less than 5 cm/s, that minor damage occurs for peak ground velocities between 5 and 14 cm/s, and that major

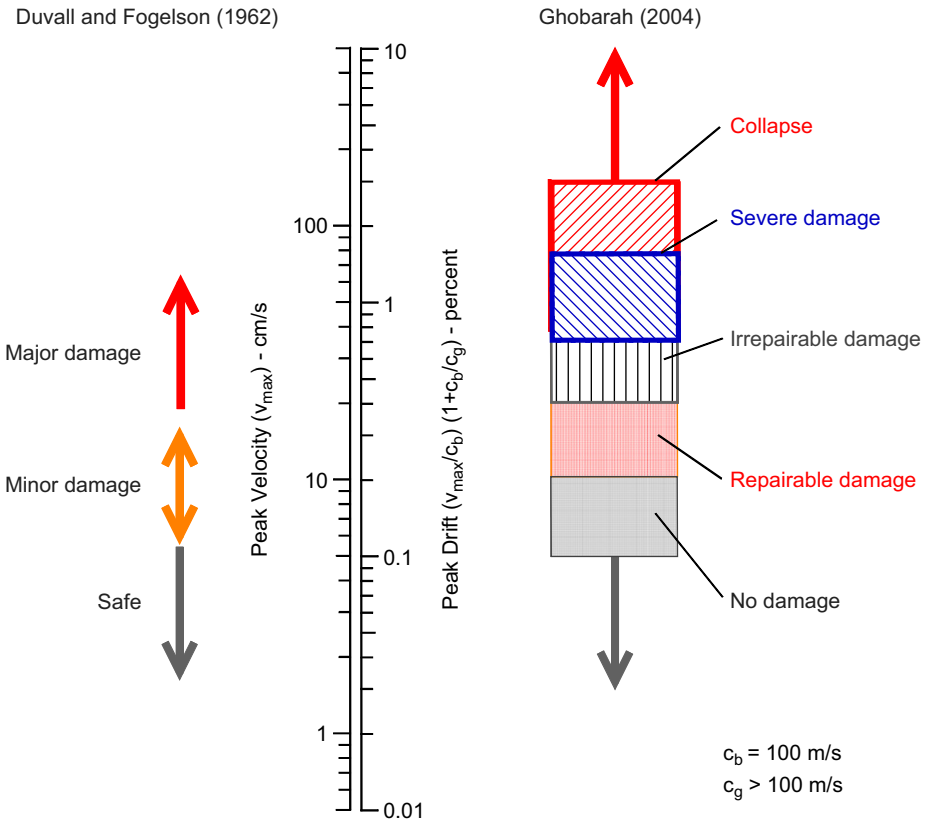

Fig. 9. Comparison of the classical empirical criteria for building damage [81] with the description of damage for five common structural systems [80] in terms of peak drifts, when a contribution of rotational excitation is considered.

damage takes place for peak velocities of about 19 cm/s and larger (Fig. 9). These velocity ranges correspond to the Modified Mercalli Intensity Levels of about V–VI, VII–VIII, and VIII–IX, respectively [82].

Depending upon the structural system, Table 5 implies collapse for drifts larger than 0.8–3.0%—that is for peak ground velocities larger than 80–300 cm/s when $c_b \ll c_g$ and 40–150 cm/s, when $c_b \sim c_g$. These two ranges of peak ground velocities are emphasized in the two right scales and by the two overlapping gray zones in Fig. 7. Detailed discussion of the observed earthquake damage, and of the trends implied by the values in Table 5, is beyond the scope of this paper, but the reader may wish to peruse the papers that describe the relationship between the observed damage and various measures of the levels of earthquake shaking following some of the earthquakes for which the geographical distribution of the strong ground motion is available and has been documented (e.g. [83–87]. This will show that the range of the observed average drifts, and of the associated consequences, as outlined in Table 5, is in good agreement with the classical simplified approach reviewed by Duval and Fogelson [81]. In Fig. 9, the right scale from Fig. 7, describing peak drifts, is shown for the assumption that the sites are on soft soils and sediments—that is when $c_b \sim c_g$—and compared with the damage criteria from Duvall and Fogelson [81] (left), and Ghobarah [80] (right).

The right scale in Fig. 7 shows that the effects of strong-motion rotation will be to amplify the relative structural response and the associated drifts by a factor between 1 and about 2 when the deformations of the structural system can be approximated by an equivalent shear beam. These estimates are based on the simplified pseudo-static interpretation of the displacements and do not include the dynamic effects, rotational waves in the buildings, and bending deformations of the overall structural system. Further research is needed to quantify those effects and to include the role of soil–structure interaction. The present qualitative analysis shows that the largest effects of rotational excitation will occur when the representative phase velocity of ground motion becomes small and comparable to the velocity of shear waves in the building.

4. Discussion and conclusions

Results of this review suggest that ignoring the contribution of the rotational components of strong motion can result in underestimated drifts (by a factor approaching about two) in the structures deforming mainly in shear. This estimate is a lower bound based only on the pseudo-static deformations of the structure, and it neglects the contributions from permanent tilting of ground surface, soil–structure interaction, dynamic effects, and the bending deformations in the structural system. Furthermore, we considered only the linear components of ground motion and of the structural response. When all of those contributions are accounted for, together with the nonlinear response of the soil and of the structure, the part of the drift that results (directly or indirectly) from strong-motion rotations may be considerably larger.

One of the aims of this paper has been to estimate the amplitudes of the linear, transient, rotational strong motion in the vicinity of the earthquake faults. With increasing distance from the source, the amplitudes of both translational and rotational components of motion will decrease due to attenuation and geometric spreading, but the factors associated with propagation through inhomogeneous media, which involve interference and focusing, may contribute to some local amplification.

The considerations in this paper are approximate and simplified not only because we included only the linear superposition of the translational and rotational effects of strong ground motion but also because we did not include the coupling of the translational and rotational motions, dynamic instability, geometric nonlinearities, and the effects of gravity forces that accompany the response of all metastable systems and that are emphasized and become more complicated when the wave passage effects are included in the analysis.

At present, the role of sudden and large initial velocities in the strong ground motion in the near field is completely ignored even in the most advanced engineering studies of the effects of the near-field motions on the response. Our examples, in terms of d_F and d_N displacements, which do include physically correct nature of the near source motions, not only include the large initial velocities but are also accompanied by sudden large rotations. Both can have profound effects on the response of structures near faults [88,89] and can dominate in both linear and nonlinear responses. When combined with the effects of propagating excitation, which result in differential excitation of columns [90], the complexity of the response of even the simplest of structures can become considerable [91].

It is hoped that this study will contribute toward recognition that the rotational components that accompany the translational earthquake ground motion are also important, that they should be recorded during future earthquakes, and that they must be included in engineering analyses of structural response.

Acknowledgment

I am indebted to two anonymous reviewers who offered detailed and valuable comments and suggestions, which resulted in significant improvements of this paper.

References

[1] Biot MA. Vibrations of building during earthquake, Chapter II. Ph.D. Thesis no. 259 entitled transient oscillations in elastic systems. Pasadena, CA: Aeronautics Department, California Institute of Technology; 1932.
[2] Biot MA. Theory of elastic systems vibrating under transient impulse with an application to earthquake-proof buildings. Proc Natl Acad Sci 1933;19(2):262–8.
[3] Biot MA. Theory of vibration of buildings during earthquake. Zeitsch Angew Mat Mech 1934;14(4):213–23.
[4] Trifunac M.D. 75th anniversary of the response spectrum method—a historical review. Soil Dyn Earthquake Eng 2008, in press, doi:10.1016/j.soildyn.2007.11.007.
[5] Biot MA. Mechanics of incremental deformation. New York: Wiley; 1965.
[6] Gičev V, Trifunac MD. Permanent deformations and strains in a shear building excited by a strong motion pulse. Soil Dyn Earthquake Eng 2007;27(8):774–92.
[7] Gičev V, Trifunac MD. Energy and power of nonlinear waves in a seven story reinforced concrete building. Indian Soc Earthquake Tech J 2007;44(1):305–23.
[8] Teisseyre R, Majewski E. Physics of earthquakes. International handbook of earthquake and engineering seismology. Part A, 2002. p. 229–35.
[9] Kharin DA, Simonov LI. VBPP seismometer for separate registration of translational motion and rotations. Seism Instrum 1969;5:51–66 [in Russian].
[10] Lee VW, Trifunac MD. Torsional accelerograms. Int J Soil Dyn Earthquake Eng 1985;4(3):132–9.
[11] Lee VW, Trifunac MD. Rocking strong earthquake accelerations. Int J Soil Dyn Earthquake Eng 1987;6(2):75–89.
[12] Niazi M. Inferred displacements, velocities and rotations of long rigid foundation located in El Centro differential array site during the 1979 Imperial Valley, California earthquake. Earthquake Eng Struct Dyn 1986;14:531–42.
[13] Graizer VM. Determination of the path of ground motion during seismic phenomena. Izv USSR Acad Sci Phys Solid Earth 1987;22(10):791–4.
[14] Graizer VM. Ob izmerenii naklona zemnoi poverhnosti vblizi epicentra vzriva. Dokladi Akademii Nauk S.S.S.R., Geofizika 1989;305(2):314–8.
[15] Graizer VM. Inertial seismometry methods. Izv USSR Acad Sci Phys Solid Earth 1991;27(1):51–61.
[16] Graizer VM. Equations of pendulum motion including rotations and its implications to the strong ground motion, Chapter 34. In: Teisseyre R, Takeo M, Majewski E, editors. Earthquake source asymmetry, structural media and rotation effects. Heidelberg, Germany: Springer; 2006. p. 471–85.
[17] Graizer VM. Tilts in strong ground motion. Bull Seism Soc Am 2006;96(6):2090–102.
[18] Nigbor RL. Sex-degree-of-freedom ground motion measurements. Bull Seism Soc Amer 1994;84(5):1665–9.
[19] Takeo M. Ground rotational motions recorded in near-source region of earthquakes. Geophys Res Lett 1998;25(6):789–92.
[20] Takeo M. Ground rotational motions recorded in near-source region of earthquakes, Chapter 12. In: Teisseyre R, Takeo M, Majewski E, editors. Earthquake source asymmetry, structural media and rotation effects. Heidelberg, Germany: Springer; 2006. p. 157–67.
[21] Huang BS. Ground rotational motions of the 1999 Chi-Chi, Taiwan earthquake as inferred from dense array observations. Geophys Res Lett 2003;30(6) Art. nos. 1307, 40-1, 40-4.
[22] Trifunac MD. Effects of torsional and rocking excitations on the response of structures, Chapter 39. In: Teisseyre R, Takeo M, Majewski E, editors. Earthquake source asymmetry, structural media and rotation effects. Heidelberg, Germany: Springer; 2006. p. 569–82.
[23] Kalkan E, Graizer V. Multi-component ground motion spectra for coupled horizontal, vertical, angular accelerations, and tilt. ISET J Earthquake Technol 2007;44(1):259–84.
[24] Kalkan E, Graizer V. Coupled tilt and translational ground motion response spectra. ASCE J Struct Eng 2007;133(5):609–19.
[25] Trifunac MD. A note on rotational components of earthquake motions for incident body waves. Soil Dyn Earthquake Eng 1982;1(1):11–9.
[26] Teisseyre R, Suchcicki J, Teisseyre K, Wiszniowski J, Palangio P. Seismic rotation waves: basic elements of theory and recording. Ann Geophys 2003;46(4):671–85.
[27] Teisseyre R, Boratynski W. Continuum with self-rotational nuclei: evolution of defect fields and equations of motion. Acta Geophys Pol 2002;50:223–30.
[28] Farrell WF. A gyroscopic seismometer: measurements during the Borrego Earthquake. Bull Seism Soc Am 1969;59(3):1239–45.
[29] Bradner H, Reichle M. Some methods for determining acceleration and tilt by use of pendulums and accelerometers. Bull Seism Soc Am 1973;63(1):1–7.
[30] Bouchon M, Aki K. Strain and rotation associated with strong ground motion in the vicinity of earthquake faults. Bull Seism Soc Am 1982;72(5):1717–38.
[31] Castellani A, Boffi G. Rotational components of the surface ground motion during an earthquake. Earthquake Eng Struct Dyn 1986;14:751–67.
[32] Castellani A, Boffi G. On the rotational components of seismic motion. Earthquake Eng Struct Dyn 1989;18:785–97.
[33] Oliveira CS, Bolt BA. Rotational components of surface strong ground motion. Earthquake Eng Struct Dyn 1989;18:517–26.
[34] Nathan ND, MacKenzie JR. Rotational components of earthquake motion. Can J Civil Eng 1975;2:430–6.
[35] Droste Z, Teisseyre R. Rotational and displacement components of ground motion as deduced from data of the azimuth system of seismographs. Publs Inst Geophys Pol Acad Sci 1976;97:157–67.
[36] Moslem K, Trifunac MD. Effects of soil–structure interaction on the response of buildings during strong earthquake ground motion. Los Angeles, CA: Department of Civil Engineering report no. CE 86-04, University of Southern California; 1986. Available from; http://www.usc.edu/dept/civil_eng/Earthquake_eng/.
[37] Trifunac MD, Todorovska MI. Recording and interpreting earthquake response of full-scale structures. In: Proceedings of the NATO advanced research workshop on strong-motion instrumentation for civil eng. structures, June 2–5, 1999. Istanbul, Turkey, Dordrecht: Kluwer Academic Publication; 2001. p. 131–55.
[38] Trifunac MD, Ivanović SS. Analysis of drifts in a seven-story reinforced concrete structure. Report no. CE 03-01. Los Angeles, CA: Department of Civil Engineering, University of Southern California; 2003. Available from; http://www.usc.edu/dept/civil_eng/Earthquake_eng/.
[39] Trifunac MD, Ivanovic SS, Todorovska MI, Novikova EI, Gladkov AP. Experimental evidence for flexibility of a building foundation supported by concrete friction piles. Soil Dyn Earthquake Eng 1999;18(3):169–87.
[40] Teisseyre R, Takeo M, Majewski E, editors. Earthquake source asymmetry, structural media and rotation effects. Berlin Heidelberg: Springer; 2006.
[41] Haskell NA. Elastic displacements in the near field of a propagating fault. Bull Seism Soc Am 1969;59:865–908.
[42] Trifunac MD. Broad band extension of fourier amplitude spectra of strong motion acceleration. Report CE 93-01. Los Angeles, CA: Department of Civil Engineering, University of Southern California; 1993. Available from; http://www.usc.edu/dept/civil_eng/Earthquake_eng/.
[43] Trifunac MD, Todorovska MI. Broadband extension of pseudo relative velocity spectra of strong motion. Report CE 94-02. Los Angeles, CA: Department of Civil Engineering, University of Southern California; 1994. Available from; http://www.usc.edu/dept/civil_eng/Earthquake_eng/.
[44] Richter CF. Elementary seismology. San Francisco: Freeman and Co.; 1958.
[45] Trifunac MD. Stresses and intermediate frequencies of strong motion acceleration. Geofizika 1998;14:1–27.
[46] Trifunac MD, Todorovska MI, Lee VW. The Rinaldi strong motion accelerogram of the Northridge, California, earthquake of 17 January 1994. Earthquake Spectra 1998;14(1):225–39.

[47] Chen K-C, Huang B-S, Wang J-H, Huang W-G, Chang T-M, Hwang R-D, et al. An observation of rupture pulses of the 20 September 1999 Chi-Chi, Taiwan, earthquake from near-field seismograms. Bull Seism Soc Am 2001;91(5): 1247–54.
[48] Todorovska MI, Trifunac MD. Impulse response analysis of the Van Nuys 7-story hotel during 11 earthquakes and earthquake damage detection. Struct Control Health Monitor 2008;15(1):90–116.
[49] Trifunac MD, Todorovska MI. Nonlinear soil response—1994 Northridge, California earthquake. J Geotech Eng, ASCE 1996;122(9):725–35.
[50] Trifunac MD, Udwadia FE. Parkfield, California, earthquake of June 27, 1966: a three-dimensional moving dislocation. Bull Seism Soc Am 1974;64(3):511–33.
[51] Trifunac MD. A three-dimensional dislocation model for the San Fernando, California earthquake of February 9, 1971. Bull Seism Soc Am 1974;64:149–72.
[52] Housner GW, Trifunac MD. Analysis of accelerograms—Parkfield earthquake. Bull Seism Soc Amer 1967;57(6):1193–220.
[53] Trifunac MD, Hudson DE. Analysis of the Pacoima Dam accelerogram, San Fernando, California earthquake of 1971. Bull Seism Soc Am 1971;61(5): 1393–411.
[54] Trifunac MD, Lee VW. Routine computer processing of strong-motion accelerograms. Pasadena, CA: Earthquake Engineering Research Laboratory, EERL 73-03, California Institute of Technology; 1973. Available from; http://www.usc.edu/dept/civil_eng/Earthquake_eng/.
[55] Trifunac MD, Lee VW. Uniformly processed strong earthquake ground accelerations in the Western United States of America for the period from 1933 to 1971: corrected acceleration, velocity and displacement curves. Report CE 78-01. Los Angeles, CA: Department of Civil Engineering, University of Southern California; 1978. Available from; http://www.usc.edu/dept/civil_eng/Earthquake_eng/.
[56] Lin CH, Lee VW, Trifunac MD. Effects of boundary drainage on the reflection of elastic waves in a poroelastic half space saturated with non-viscous fluid. Report no. CE 01-04. Los Angeles, CA: Department of Civil Engineering University of Southern California; 2001. Available from; http://www.usc.edu/dept/civil_eng/Earthquake_eng/.
[57] Sanchez-Sesma FJ, Palencia VJ, Luzon F. Estimation of local site effects during earthquakes: an overview. Indian Soc Earthquake Technol J 2002;39(3): 167–94.
[58] Trifunac MD. Stress estimates for San Fernando, California earthquake of February 9, 1971: main event and thirteen aftershocks. Bull Seism Soc Am 1972a;62(3):721–50.
[59] Takeo M, Ito HI. What can be learned from rotational motions excited by earthquakes? Geophys J Int 1997;129:319–29.
[60] Trifunac MD, Todorovska. Tsunami source parameters of submarine earthquakes and slides. In: Locat J, Mienert J, editors. In: Proceeding of the first international symposium on submarine mass movements and their consequences. EGS-AGU-EUG joint meeting, Nice, France, April 7–11. Kluwer Academic Publishers; 2003. p. 121–8.
[61] Trifunac MD. Buildings as sources of rotational waves, Chapter I.5. In: Teisseyre R, Nagahama H, Majewski E, editors. Physics of asymmetric continua: extreme and fracture processes. Heidelberg, Germany: Springer; 2008 [in press].
[62] Sezawa K, Kanai K. Decay in the seismic vibration of a simple or tall structure by dissipation of their energy into the ground. Bull Earth Res Inst 1935; XIII(3):681–97.
[63] Sezawa K, Kanai K. Improved theory of energy dissipation in seismic vibrations on a structure. Bull Earth Res Inst 1936;XIV(2):164–8.
[64] Biot MA. Influence of foundation on motion of blocks. Soil Dyn Earthquake Eng 2006;26(6–7):486–90.
[65] Trifunac MD. A method for synthesizing realistic strong ground motion. Bull Seism Soc Am 1971;61(6):1739–53.
[66] Wong HL, Trifunac MD. Generation of artificial strong-motion accelerograms. Earthquake Eng Struct Dyn 1979;7(6):509–27.
[67] Lee VW. Surface strains associated with strong earthquake shaking. JSCE 1990;422(1–14):187–94.
[68] Trifunac MD. Curvograms of strong ground motion. ASCE, J Eng Mech Div 1990;116(6):1426–32.
[69] Newmark NM. Torsion in symmetrical buildings. In: Proceedings of the 4th world conference on earthquake engineering, Santiago, Chile, 1969. p. A3.19–32.
[70] Trifunac MD, Todorovska MI. A note on the useable dynamic range of accelerographs' recording translation. Soil Dyn Earthquake Eng 2001;21(4): 275–86.
[71] Yuan SW. Foundations of fluid mechanics. Englewood Cliffs, NJ: Prentice-Hall Inc.; 1967.
[72] Trifunac MD, Novikova EI. Duration of earthquake fault motion in California. Earthquake Eng Struct Dyn 1995;24(6):781–99.
[73] Trifunac MD. Preliminary analysis of the peaks of strong earthquake ground motion-dependence of peaks on earthquake magnitude, epicentral distance and the recording site conditions. Bull Seism Soc Am 1976;66(1): 189–219.
[74] Gupta VK, Trifunac MD. Investigation of building response to translational and rotational earthquake excitations. Report CE 89-02. Los Angeles, CA: Department of Civil Engineering, University of Southern California; 1989. Available from: http://www.usc.edu/dept/civil_eng/Earthquake_eng/.
[75] Todorovska MI, Lee VW. Seismic waves in buildings with shear walls or central core. J Eng Mech, ASCE 1989;115(12):2669–86.
[76] Todorovska MI, Trifunac MD. Propagation of earthquake waves in buildings with soft first floor. J Eng Mech, ASCE 1990;116(4):892–900.
[77] Todorovska MI, Trifunac MD. A note on excitation of long structures by ground waves. J Eng Mech, ASCE 1990;116(4):952–64.
[78] Trifunac MD, Todorovska MI. Response spectra and differential motion of columns. Earthquake Eng Struct Dyn 1997;26(2):251–68.
[79] Trifunac MD, Gičev V. Response spectra for differential motion of columns. Paper II: Out-of-plane response. Soil Dyn Earthquake Eng 2006;26(12): 1149–60.
[80] Ghobarah A. On drift limits associated with different damage levels. In: Proceedings of the international workshop on performance-based seismic design. Bled, Slovenia, 2004. p. 321–32.
[81] Duvall WI, Fogelson DE. Review of criteria for estimating damage to residences from blasting vibrations. US Department of the Interior, Bureau of Mines. Report of investigations 5968, 1962.
[82] Trifunac MD, Brady AG. On the correlation of seismic intensity scales with the peaks of recorded strong ground motion. Bull Seism Soc Am 1975;65(1): 139–62.
[83] Trifunac MD. Nonlinear soil response as a natural passive isolation mechanism. Paper II—The 1933 Long Beach, California earthquake. Soil Dyn Earthquake Eng 2003;23(7):549–62.
[84] Trifunac MD, Todorovska MI. Northridge, California, earthquake of 1994: density of red-tagged buildings versus peak horizontal velocity and intensity of shaking. Soil Dyn Earthquake Eng 1997;16(3):209–22.
[85] Trifunac MD, Todorovska MI. Nonlinear soil response as a natural passive isolation mechanism—the 1994 Northridge, California earthquake. Soil Dyn Earthquake Eng 1998;17(1):41–51.
[86] Trifunac MD, Todorovska MI. Reduction of structural damage by nonlinear soil response. J Struct Eng, ASCE 1998;125(1):89–97.
[87] Trifunac MD, Todorovska MI. Long period microtremors, microseisms and earthquake damage: Northridge, California earthquake of 17 January 1994. Soil Dyn Earthquake Eng 2000;19(4):253–67.
[88] Jalali R, Trifunac MD, Ghodrati Amiri G, Zahedi M. Wave-passage effects on strength-reduction factors for design of structures near earthquake faults. Soil Dyn Earthquake Eng 2007;27(8):703–11.
[89] Jalali R, Trifunac MD. A note on strength reduction factors for design of structures near earthquake faults. Soil Dyn Earthquake Eng 2008;28(3): 212–22.
[90] Trifunac MD. Differential earthquake motion of building foundations. J Struct Eng, ASCE 1997;4:414–22.
[91] Jalali R, Trifunac MD. Strength-reduction factors for structures subjected to differential near-source ground motion. Indian Soc Earthquake Technol J 2007;44(1):285–304.
[92] Fletcher J, Boatwright J, Haar L, Hanks T, McGarr A. Source parameters for aftershocks of the Oroville, California, earthquake. Bull Seism Soc Am 1984;74(4):1101–23.
[93] Trifunac MD. Tectonic stress and source mechanism of the Imperial Valley, California earthquake of 1940. Bull Seism Soc Am 1972b;62(5):1283–302.
[94] Trifunac MD. Nonlinear problems in earthquake engineering. In: Springer's encyclopedia of complexity and system science, 2008 [in press].